NANOSYSTEMS:
PHYSICS, CHEMISTRY, MATHEMATICS

Yeletsky P.M., et al. *Nanosystems: Phys. Chem. Math.*, 2024, **15** (2), 285–299.
http://nanojournal.ifmo.ru
DOI 10.17586/2220-8054-2024-15-2-285-299

Original article

Green approach to production of porous char adsorbents via oxidative carbonization in fluidized catalyst bed

Petr M. Yeletsky, Nikolay A. Yazykov, Yury V. Dubinin, Maksim M. Borodaevskiy, Svetlana A. Selishcheva, Vadim A. Yakovlev

Federal Research Center Boreskov Institute of Catalysis SB RAS, Novosibirsk, Russia

Corresponding author: Petr M. Yeletsky, yeletsky@catalysis.ru

ABSTRACT A green and energy-efficient technique for production of porous carbon-mineral chars from agricultural wastes (rice husk, wheat bran) and sedimentary carbonaceous feedstocks (high-ash peat, coal) was developed. It is based on partial combustion in fluidized bed of a deep oxidation catalyst at low temperatures (465 – 600 °C). This technique yields porous chars with an elevated mineral content that depends on a feedstock used, and gaseous products of complete oxidation. It was found that the obtained chars have developed porosity with BET specific surface area of *ca.* 50 – 170 m^2g^{-1}, pore volume of 0.05 – 0.17 $ml{\cdot}g^{-1}$, and ash content of 16 – 79 wt. %. They were additionally characterized by TGA and FTIR. Their testing as adsorbents for heavy metal ions (by the example of Cu^{2+}) and organic dyes (by the example of methyl green) revealed that their adsorption capacities are comparable to those of chars produced by the conventional pyrolytic approaches.

KEYWORDS biochar, biomass, rice husk, bran, fluidized catalyst bed, composite

ACKNOWLEDGEMENTS The work was supported by the Ministry of Science and Higher Education of the Russian Federation within the governmental order for Boreskov Institute of Catalysis (project FWUR-2024-0038). The authors also thank Dr. Roman B. Tabakaev from University of Tyumen for providing feedstock (wheat bran and high-ash peat).

FOR CITATION Yeletsky P.M., Yazykov N.A., Dubinin Y.V., Borodaevskiy M.M., Selishcheva S.A., Yakovlev V.A. Green approach to production of porous char adsorbents via oxidative carbonization in fluidized catalyst bed. *Nanosystems: Phys. Chem. Math.*, 2024, **15** (2), 285–299.

1. Introduction

Nowadays, a lot of literature is devoted to the study of various processes of conversion of plant biomass to obtain solid carbonaceous products (biochar) that find applications in many fields of science and technology. Biochar is considered as a cheap environmentally friendly adsorbent with a developed porous structure and a high content of oxygen-containing surface functional groups. In addition, it also used to increase soil fertility and for remediation, for wastewater treatment, as a feedstock for activated carbons, as well as an energy carrier with a higher calorific value and density than the feedstock [1, 2]. Biochar from plant biomass can be obtained by gasification [3], hydrothermal carbonization [4] as well as various types of pyrolysis – torrefaction [5], slow and fast pyrolysis with both the conventional heating [6, 7], and microwave one [8]. Almost all of the above approaches are characterized by the need to create an environment (e.g., inert or aqueous) as well as supplying energy on the heating. Currently, pyrolysis is considered to be a more attractive process for obtaining these materials. Depending on the process time together with the temperature, this approach can be divided into the following types: slow ($t = 5$ – 30 min at $T = 300$ – 600 °C), intermediate ($t = 10$ – 30 s at $T = 500$ – 600 °C), fast ($t < 2$ s, at $T = 450$ – 600 °C) and flash pyrolysis ($t < 0.5$ s at $T = 800$ – 1000 °C) [9]. The last two types of pyrolysis are usually carried out in a fluidized bed of a heat carrier, which is usually quartz sand. Particles of raw materials are suspended in a fluidized bed of a heated heat carrier, due to which the intense heat and mass transfer is attained. These properties of the fluidized bed make it suitable for the processing of particulate feedstock. In addition, processes using fluidized bed reactors are very flexible in terms of feed calorific value, moisture content, particle size, density and heteroatom content [10]. A significant increase in the efficacy of this process can be achieved by carrying it out in the presence of oxygen, as well as using particles of a catalyst instead of the sand. Partial oxidation allows the process to be carried out in an auto- or exothermic mode, i.e. to reduce power inputs, or even – to receive heat energy, and the use of catalysts – more efficiently control the process direction [11]. However, currently, catalysts are rarely used for biomass pyrolysis in a fluidized bed. Except zeolite ZSM-5 that utilized to increase the yield of fast pyrolysis oil [11, 12], there are practically no other examples of utilization of catalysts of other formulations. Therefore, the search and application of more suitable and stable catalytic systems is urgent.

At the Boreskov Institute of Catalysis, the technology based combustion in a fluidized bed of a deep oxidation catalysts has been developed, that was successfully tested for combustion of various fuels [13, 14], including such difficult

to utilize ones like shale heavy coal-tar products [15], heavy high-sulfuric oils [16,17], as well as sewage sludge [18]. The use of the deep oxidation catalyst for fuel combustion allows heat production and extraction to be carried out within the same fluidized bed at a near stoichiometric air-to-fuel ratio. Furthermore, this technology can be related to truly green, since:

- all the combustion products are being practically completely oxidized to CO_2 and water, with a content of harmful substances within the Environmental Standards;
- allows for reduction of combustion temperature from 800 – 1000 °C to 450 – 750 °C, thus diminishing requirements to heat resistance of the construction materials, as well as avoiding the high-temperature NOx formation.

Thus, all the above advantages make this technology suitable for clean, facile and energy-efficient production of char from biomass and other carbon-containing feedstocks [19].

Recently, in the previous work, a set of chars from two biomass wastes (wheat bran and rice husk) as well as two sedimentary feedstocks (highly-mineralized peat, and coal) were obtained via partial combustion in the fluidized catalyst bed (FCB) reactor at 465 – 600 °C and evaluated as precursors of porous carbons via acid leaching of the char mineral phase [20]. The goal of this work is to investigate the obtained materials with a wider set of characterization techniques that include FTIR and TGA, as well as estimate properties of the synthesized chars as potential adsorbents for wastewater treatment through the removal of inorganic and organic industrial pollutants. As such pollutants, heavy metal ions (by the example of Cu^{2+}) and organic dyes (by the example of methyl green) were selected.

2. Material and methods

2.1. Feedstock carbonization in reactor with fluidized catalyst bed

For the study, the following feedstocks have been used: 1) wheat bran (WB) obtained from Kemerovo region (Russia); 2) rice husk (RH, Krasnodar region, Russia); 3) highly mineralized peat Sukhovskoy from deposit Sukhovskoye (Tomsk region, Russia); 4) coal, grade DOMSSH from "Vinogradovsky" coal mine (Kemerovo region, Russia). The composition of the feedstocks, including their mineral component, is provided in Tables 1 – 2. The properties of the used WB are presented in more detail in [21], peat Sukhovskoy – in [22], and RH – in [23].

TABLE 1. Composition of the used feedstocks

Feedstock	$W^{a\,1}$, wt. %	$A^{d\,2}$, wt. %	$V^{daf\,3}$, wt. %	$FC^{daf\,4}$, wt. %	CHNS-O-composition, wt. %				
					C^{daf}	H^{daf}	N^{daf}	S^{daf}	$O^{daf\,5}$
WB	8.6	6.9	81.0	12.1	49.14	6.66	3.30	0.07	40.83
RH	5.0	19.5	65.0	15.5	51.55	6.83	0.06	0.02	41.54
Peat	9.9	22.8	74.8	2.4	52.06	6.31	3.58	0.20	37.85
Coal	14.9	8.3	35.8	55.9	77.09	5.43	1.98	0.95	14.55

[1] – moisture content; [2] – ash content on dry matter; [3] – volatile matter; [4] – fixed carbon; [5] – calculated by difference

TABLE 2. Composition of ash of the used feedstocks in recalculation to oxides of the corresponding elements (wt. %). WB and peat – according to the results of energy dispersive X-ray fluorescence (EDXRF) [21], RH – according to ICP-OES [23]; and coal – provided by the supplier

Feedstock	SiO_2	Al_2O_3	Fe_2O_3	CaO	MgO	Na_2O	K_2O	TiO_2	Mn_2O_3	P_2O_5	SO_3
WB	1.74	26.3	0.41	0.93	16.3	28.6	17.9	–	–	7.9	–
RH	95.8	0.11	0.12	1.06	0.33	0.3	2.17	–	0.08	–	–
Peat	3.8	6.85	8.53	39.8	11.1	23.2	0.26	–	–	6.51	–
Coal	54.4	23.8	7.07	5.44	1.34	0.44	1.39	1.1	0.07	0.95	4

The previous studies have shown that mineral component of WB and RH is X-Ray amorphous, while those of coal includes quartz and those of peat contains $CaCO_3$ and CaO [20].

Carbonization of the feedstocks in air flow was carried out using the laboratory installation set up equipped by the fluidized catalyst bed reactor with a deep oxidation catalyst (Fig. 1). The catalyst was supplied by the Engineering Center of the Boreskov Institute of Catalysis and represents $CuO–Cr_2O_3/\gamma$-Al_2O_3 spherical particles with a diameter of 1.5 –

2.0 mm and contain Cr_2O_3 – 6.5 wt. % + CuO – 3.5 wt. %. Its BET specific surface area is 115 m^2g^{-1}, pore volume – 0.3 $ml \cdot g^{-1}$ and mean pore size – 10.5 nm. The installation includes a feedstock tank, from which, via of a screw driver, a feedstock is fed into a fluidized bed reactor. All the raw materials were previously ground to a particle size less than 1 mm. The FCB reactor is 75 mm i.d. and loaded with 1000 mm of the height of the fluidized catalyst bed ($\sim$ 3.5 L in volume). Preheated airflow is supplied to the bottom of the reactor and controlled by rotameters. After the reactor outlet, the carbonized feedstock is separated from the exhaust in the cyclone and falls into the collecting tank. Carbonization trials were carried out in isothermal mode along with the bed height.

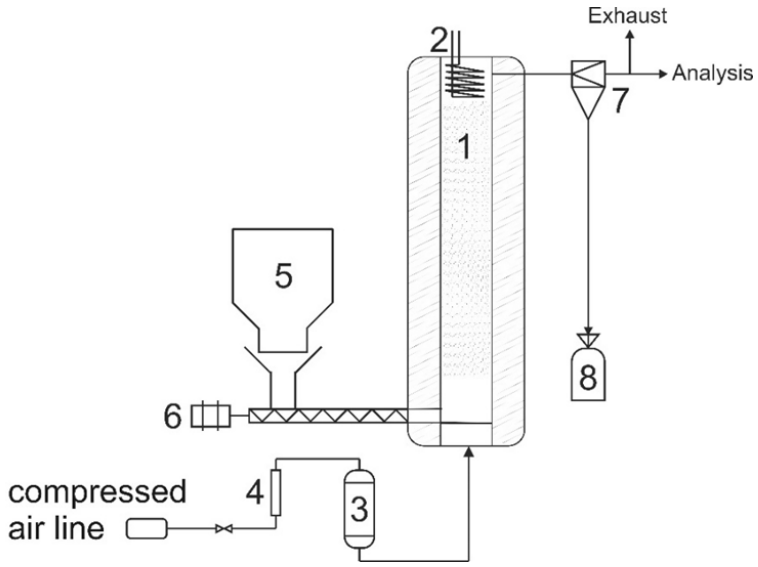

FIG. 1. A scheme of laboratory installation for combustion of solid fuels in a fluidized bed of catalyst. 1 – reactor; 2 – heat exchanger; 3 – electric air heater; 4 – rotameter; 5 – feedstock tank; 6 – screw feeder; 7 – cyclone; 8 – carbonized feedstock collection tank

Sample designations: feedstocks combusted in the FCB reactor are designated as "XTTT", where "X" is the abbreviation of a feedstock (X = P – peat, C – coal, B – wheat bran, and RH – rice husk) and "TTT" designates the carbonization temperature – 465, 550 or 600 °C.

2.2. Characterization techniques

The elemental composition of samples was determined by means of a VARIO EL CUBE CHNS analyzer (Elementar Analysensysteme GmbH, Germany).

The porous structure of the chars was characterized with nitrogen adsorption at 77 K. Nitrogen adsorption isotherms were measured by a surface area and pore size analyzer Autosorb 6B (Quantachrome Instruments, Austria). Before the measurements, all the samples were degassed under vacuum to remove moisture and other adsorbed contaminations. The char samples were pretreated at 150 °C for 4 h. The specific surface area was calculated by the standard BET method according to IUPAC recommendations [24], micropore volume was estimated by the α_S-plot method using the non-porous carbon Cabot BP 280 as a reference material [25]. The differential pore size distributions (PSD) were computed by means of Quenched Solid Density Functional Theory Method (QSDFT) equilibrium model for nitrogen adsorption at 77 K in cylinder-like pores of carbon, applied to the adsorption branch of an isotherm, using software supplied with the above instrument.

Samples of the chars were investigated by FTIR spectroscopy using a Bruker Alpha II spectrometer equipped the Platinum Diamond ATR unit (Bruker, USA), in the diapason of 400 – 4000 cm^{-1} with a resolution of 4 cm^{-1} and accumulation of 32 scans.

Synchronous thermal analysis (STA), which includes simultaneous thermogravimetric determination (TG) of differential scanning calorimetry (DSC) and mass spectrometric analysis of the recovered gas (ABG-MS), was performed on a STA 449F1 Jupiter® instrument combined with a quadrupole mass-spectrometer QMS 403D Aëolos® (NETZSCH, Germany). The experiments were carried out using a high-temperature furnace with a graphite heater and water cooling. We used a measuring sensor DSC/TG Cp S TC: type S (0 . . . 1650 °C). The experiments were carried out in open Al_2O_3 crucibles, within a temperature range of 30 – 900 °C, in the Ar atmosphere with the heating rate of 10 °C/min, and the Ar flow rate of 20 ml/min. The processing of the experimental data was carried out using the Proteus analysis software package (NETZCH, Germany).

2.3. Adsorption tests by methyl green and Cu^{2+}

As model pollutants, aqueous solutions of methyl green (MG, Fig. 2) with an initial concentration of 0.019 $g \cdot L^{-1}$ and copper sulfate with a concentration of copper ions of 0.20 $g \cdot L^{-1}$ were used.

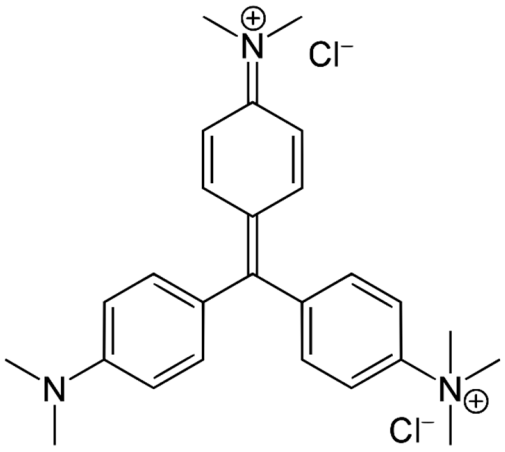

FIG. 2. Structure formula of methyl green

The experiments were carried out in glass vials with a volume of 35 ml. Acidity of the medium during the adsorption was controlled using a buffer solution with pH = 4. A weighed portion of a sorbent (15 mg) was added to a solution with the known concentration, followed by leaving the mixture without access to the light for a specified period of time. Upon the process finishing, an adsorbent was separated on a paper filter. The contaminant concentration in the filtrate was measured by visible spectrophotometry on a Cary 300 instrument (Agilent Technologies Inc., USA) in quartz cuvettes with an optical path length of 1.0 cm. The following extinction coefficients were determined in the calibration tests: $4.08 \cdot 10^1$ $L \cdot g^{-1} cm^{-1}$ for MG (632 nm); and $5.00 \cdot 10^1$ $L \cdot g^{-1} cm^{-1}$ for copper ions (805 nm). When determining the adsorption capacity, solutions with a volume of 25 ml were left for a week.

3. Results and discussion

Carbonization of biomass and sedimentary feedstocks in fluidized catalyst bed reactor allowed for obtaining of a set of porous carbon-mineral char samples. Their yields and ash contents (used as the basis for calculation of the yields) are presented in Fig. 3.

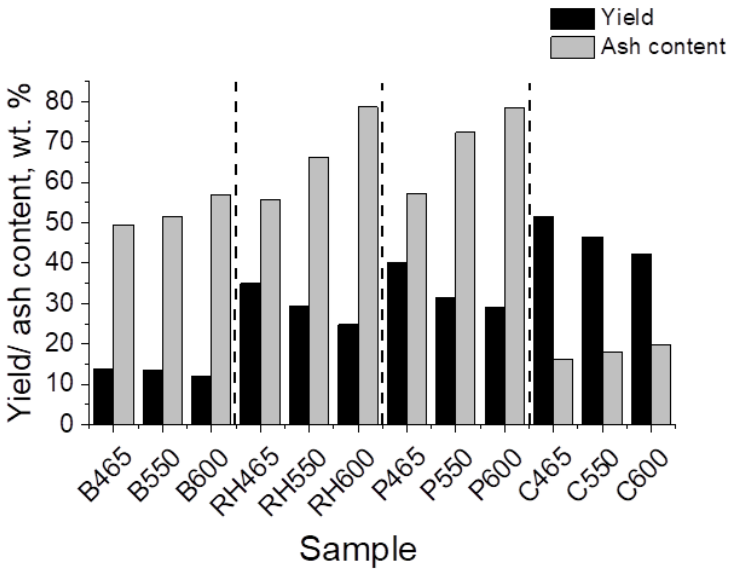

FIG. 3. Yield and ash content of chars from the feedstock carbonized in FCB reactor at 465 – 600 °C

As can be seen, in all the cases, as expected, with the temperature increase, yield of chars from every feedstock drops and mineral phase content increases. Carbonization of wheat bran in the fluidized catalyst bed resulted in the lowest

yield of the chars compared to other feedstocks. This can be caused by such factors as a low content of fixed carbon (12.1 wt. %) and the highest contents of alkaline metals ($>$ 46 wt. %, in the recalculation to oxides) well-known as gasification catalysts [26, 27]. Furthermore, the high content of dispersed alumina (26.3 wt. %) can also contribute to gasification via facilitating processes of cracking of the biopolymers [28].

For RH, yields of the biochar are significantly higher that seems to be due to the initially high content of the mineral component (19.5 wt. %) consisting mainly of pure silica, which does not exhibit any notable catalytic activity in the carbonization conditions. This SiO_2 forms a rigid mineral matrix hindering the diffusion of volatile carbonization products, making them to transform inside RH particles.

Yields and ash contents in carbonized peat are similar to RH despite it has the lowest fixed carbon content and a high content of Na. This can also be caused by the initially high ash content (22.8 wt. %) comparable to those of RH, and the same probable diffusion limitations for volatile oxidative pyrolysis products from the feedstock particles, thus, leading to the pyrolysis processes inside the solid feedstock particles.

For the coal, the highest yields with the lowest ash contents are observed. At the similar to WB ash content, coal contains the highest fixed carbon content (*ca.* 56 wt. %) due to the highest maturation degree. Thus, the carbon-containing phase of the coal can be characterized by the highest stability to both pyrolysis and oxidation that results in the lowest burn off degree compared to other raw materials. For example, it was previously found that another feedstock, having similar composition of carbon-containing phase – petroleum coke, was impossible to be burnt completely in the fluidized catalyst bed reactor even at 750 °C using similar deep oxidation catalyst [29].

The obtained chars were characterized by the following techniques.

3.1. Low-temperature nitrogen adsorption

BET specific surface area, and total pore volume of the samples are presented in Fig. 4 (in more detail, texture characteristics are provided in Table A1), their nitrogen adsorption isotherms and pore size distributions are shown in Figs. 5 – 8. In the case of wheat bran, the porous chars were found to have BET specific surface area (A_{BET}) of ca. 40 – 90 m^2g^{-1} and predominantly mesoporous texture (Fig. 5).

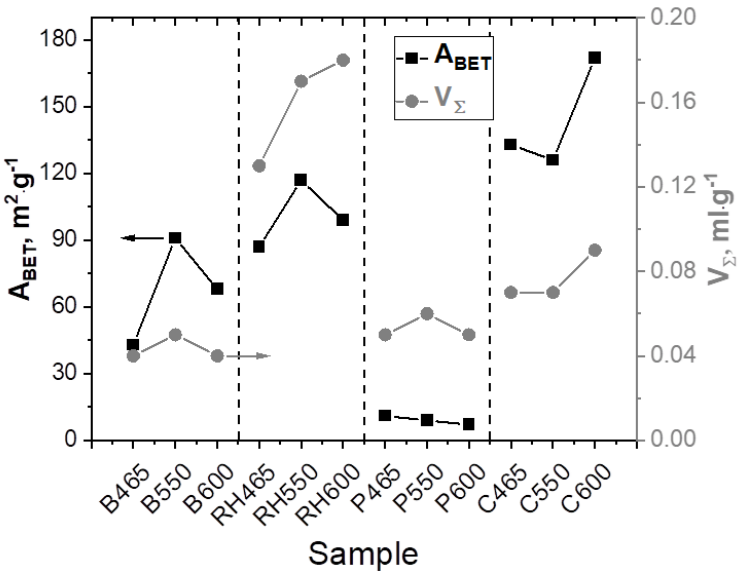

FIG. 4. A_{BET} and total pore volume of char samples from wheat bran (B465 – B600), rice husk (RH465 – RH600), peat (P465 – P600) and coal (C465 – C600) obtained via carbonization in FCB reactor at 465 – 600 °C

The nitrogen adsorption isotherms can be related to Type II [30], they indicate the presence of meso- and macropores in the samples. Their desorption branches, as can be seen, do not follow the adsorption ones most probably due to the phenomenon of swelling and/or deformation [31]. The maximally developed porosity of the sample obtained at 550 °C can be explained by the fact that it mainly depends on the carbon phase porosity, which is, probably, not developed enough at the lowest temperature, and at 600 °C the effect of mineral phase seems to dominate. The carbon-silica biochar samples from RH have more mesoporous structure (Fig. 6). Nitrogen adsorption isotherms appeared to be similar to those of WB, including the swelling effect.

The char samples have A_{BET} of *ca.* 90 – 120 m^2g^{-1} and a high pore volume of 0.13 – 0.18 cm^3g^{-1}. In this case, their A_{BET} values are also maximal at 550 °C. However, unlike bran, they are higher and closer, probably due to the greater dispersity of the silica phase, which is less prone to sintering due to the high purity, and with an increase in its contribution at 600 °C, A_{BET} also decreases, but to a lesser extent.

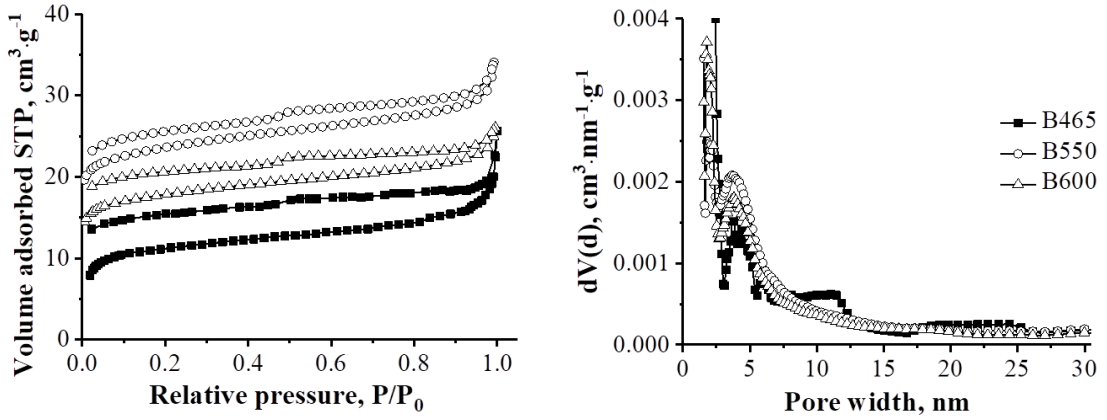

(a) (b)

FIG. 5. Nitrogen adsorption isotherms (a) and differential pore size distributions (b) on biochars obtained from wheat bran via carbonization in the FCB reactor at 465 – 600 °C

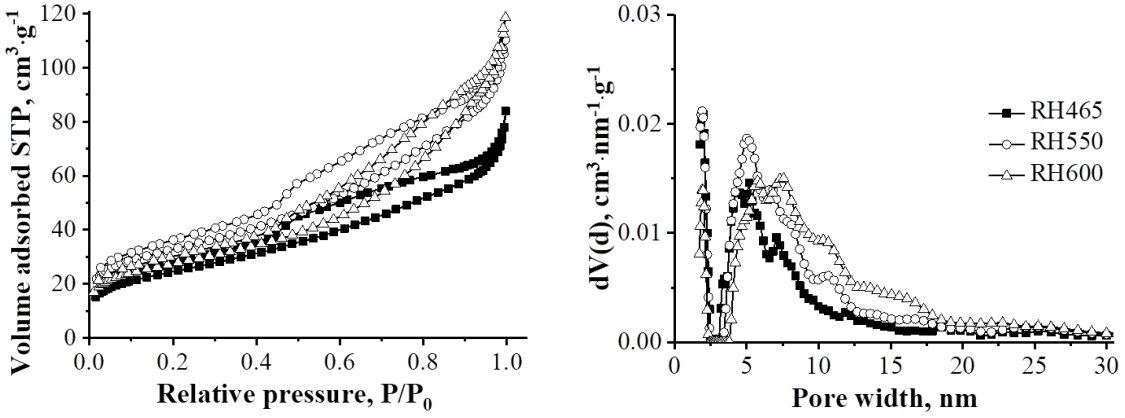

(a) (b)

FIG. 6. Nitrogen adsorption isotherms (a) and differential pore size distributions (b) on biochars obtained from rice husk via carbonization in the FCB reactor at 465 – 600 °C

Peat-derived chars were found to be mesoporous and having a low A_{BET} (*ca.* 10 m^{2}g^{-1}). The adsorption isotherms are close to Type III [30], indicating on a poorly developed porosity and the presence of large mesopores (Fig. 7). This, probably, points on the fact that the carbon-containing phase is burnt out/decomposed around the mineral phase particles evenly, without porous structure development. The mineral phase is composed of large non-porous particles that seem to be practically not contributing to the porosity. Furthermore, the low-developed porosity can be connected with the fact that unlike biomass feedstocks, carbon-containing phase of peat is represented by partially repolymerized components of biomass practically not forming porous structure during carbonization, only gasifying and burning out without a significant pore formation.

Coal-derived char samples appeared to have significantly different textural properties. Nitrogen adsorption isotherms and differential PSD of the samples are presented in Fig. 8. They indicate that the chars are microporous and exhibit the adsorption isotherms of Type I [30]. Similar texture characteristics of samples obtained at 465 and 550 °C, and the eminent properties of the char obtained at 600 °C can be connected with a high degree of maturation of the coal carbon-containing phase that stable to the oxidative treatment in the carbonization conditions.

Thus, the porosity development in the carbon-derived char samples is predominantly occurred due to burning off the most active, least matured fragments of the carbon-containing phase, resulted in the development mainly of microporosity.

3.2. FTIR spectroscopy

FTIR spectra of the studied chars are presented in Fig. 9. The spectra of WB-derived samples (Fig. 9a) include absorption bands of SiO_2 at 490, 880 and 1118 cm^{-1} corresponding to the bending vibration of O–Si–O, symmetric and asymmetric components of the stretching vibration of Si–O–Si, respectively [32]. Furthermore, the spectra show a band

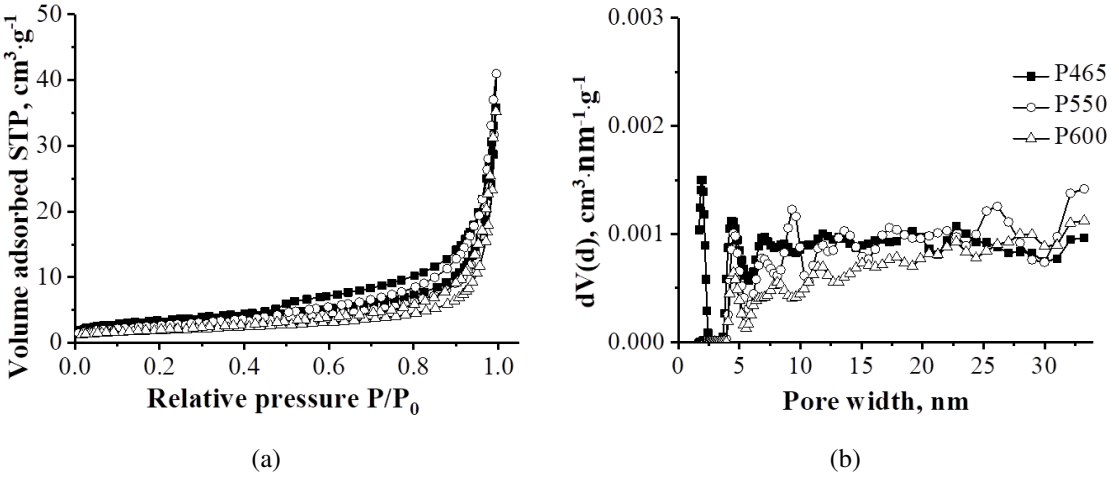

FIG. 7. Nitrogen adsorption isotherms (a) and differential pore size distributions (b) on chars obtained from Sukhovskoy highly-mineralized peat carbonized in the FCB reactor at 465 – 600 °C

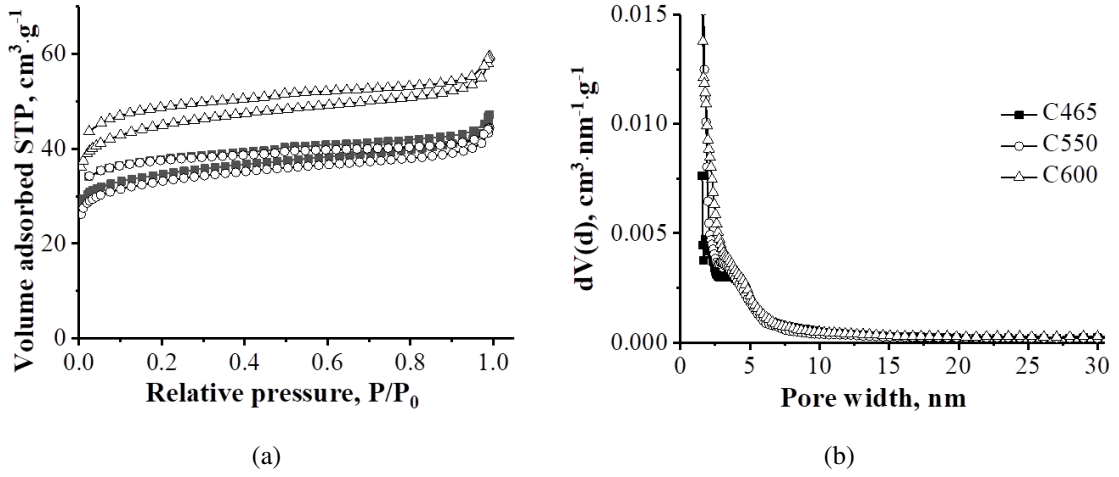

FIG. 8. Nitrogen adsorption isotherms (a) and differential pore size distributions (b) of coal carbonized in the FCB reactor at 465 – 600 °C

at 750 cm^{-1}, which can be attributed to the symmetric stretching vibrations of Si–O–Al, characteristic of aluminosilicates [33, 34]. The bands corresponding to Al–O vibrations of alumina (554 and 915 cm^{-1} for aluminum in tetrahedral and octahedral positions, respectively), in this case overlap with other bands in this region. The band at 1580 cm^{-1} may refer to C=C stretching vibrations [35].

FTIR spectra of the RH-derived biochars (Fig. 9b) also exhibit absorption bands characteristic of silica. The bands at 450 and 1055 cm^{-1} characterize the bending vibration of O–Si–O in the SiO_4 tetrahedron and the asymmetric stretching vibration of Si–O (Si), respectively, and the band at 793 cm^{-1} is a superposition of bands corresponding to the symmetric stretching vibration of Si–O–Si and vibrations of silanol Si–OH and siloxane Si–O–Si–OH groups [36, 37]. The broad low-intensity band in the region of 3000 – 3750 cm^{-1} refers to the vibrations of hydrogen-bonded OH-groups formed by silanol Si–OH groups and OH-groups of water adsorbed on the surface. For the RH600 sample, this band is the least pronounced in intensity. The band at 1593 cm^{-1} can also be referred to C=C stretching vibrations [35].

For the peat-derived chars (Fig. 10a), a number of intense bands characteristic of calcium carbonate are observed [38]. The bands at 713 and 873 cm^{-1} refer to bending CO_3^{2-} vibrations, and the bands at 1040 and 1410 cm^{-1} to symmetric and asymmetric stretching C–O vibrations within the CO_3^{2-} fragment [39].

For the FTIR spectra of coal (Fig. 10b), the absorption bands of silica are also observed. The band at 460 cm^{-1}, corresponding to bending vibration of O–Si–O in the silicate tetrahedrons, two bands in the area of 780 – 800 cm^{-1}, associated with symmetric stretching Si–O–Si vibrations, and the band near 1030 cm^{-1}, characterizing asymmetric symmetric stretching Si–O–Si vibrations [32, 40]. A doublet in the range of 780 – 800 cm^{-1} is characteristic of the low-temperature type of quartz [38]. The band at 1580 cm^{-1} can be attributed to C=C stretching vibrations in polyaromatic compounds [35].

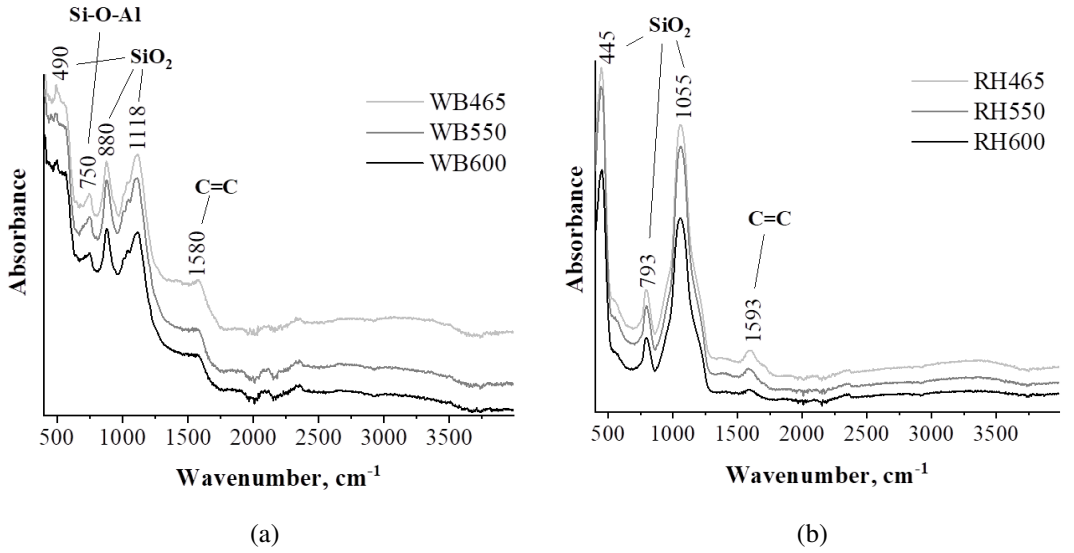

FIG. 9. FTIR spectra of WB (a) and RH (b) carbonized in fluidized catalyst bed reactor at 465 – 600 °C

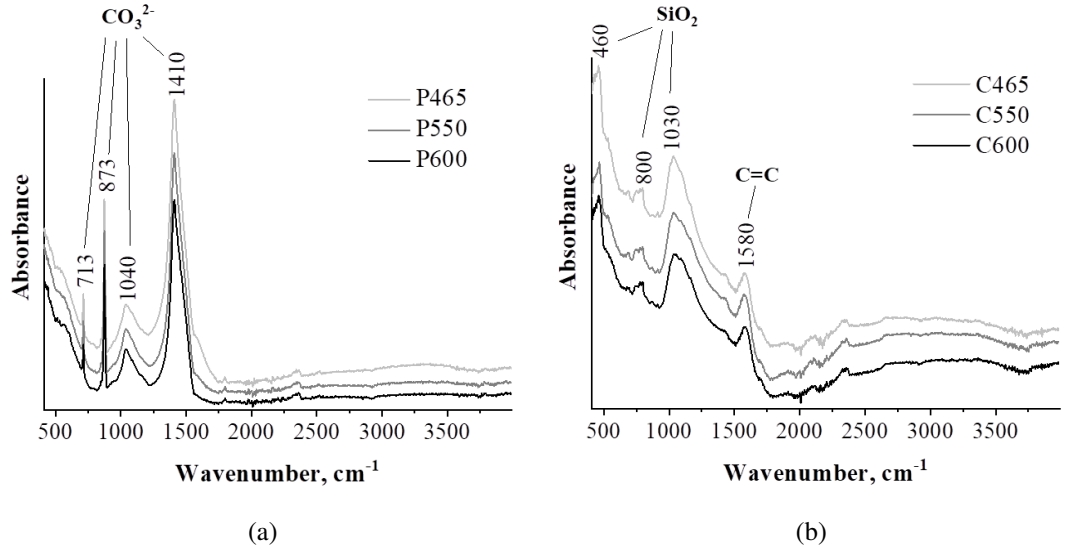

FIG. 10. FTIR spectra of peat (a) and coal (b) carbonized in fluidized catalyst bed reactor at 465 – 600 °C

3.3. TGA

Thermogravimetric and differentiating scanning calorimetry (DSC) profiles of the studied chars are provided in Appendix in Figs. A1–A4. For all samples, the thermal stability directly depends on the carbonization temperature: with the temperature increase, the weight loss decreases down. Samples obtained at 465 °C are characterized by distinctively high weight losses caused by the presence in their composition of incompletely transformed organic compounds, including polymers. The losses up to 200 – 250 °C for all samples are connected with water desorption. For biochars, the weight loss in the region of 250 – 600 °C is related to decomposition of cellulose, hemicellulose and lignin. The weight losses after *ca*. 800 °C for WB-derived chars are probably caused by the gasification of carbon-containing phase via interaction with compounds of Na and K (most probably, carbonates) constituting WB ash by *ca*. a half [23, 41]. In the case of peat-derived samples, the peaks in DSC profiles at $T > 750$ °C seems to be caused by $CaCO_3$ decomposition [42].

The most stable chars appeared to be RH600 with the minimal weight loss of 8.3 wt. % and RH550 (11.63 wt. %), while the lowest thermal stability was exhibited by peat-derived samples with the weight losses in the interval of 23.71 – 35.29 wt. %. It is also notable, the profiles of coal-derived chars exhibited the highest similarity between each other, which, apparently, is related to the highest maturation degree of the carbon-containing phase compared to other feedstocks. Their weight losses were close and relatively low – 14.5 – 16.4 wt. %.

3.4. Adsorption tests of the chars by Cu^{2+} ions and methyl green

Adsorption capacities of the char samples are provided in Fig. 11. They were calculated according to the following equation:

$$\Gamma = (C_0 - C) \cdot \frac{V}{m_{char}},$$

where Γ is the adsorption capacity (mg·g^{-1}); C_0, C is the concentration of a model pollutant in a solution (mg·L^{-1}); V is the volume of solution (L); m_{char} is the weight of the used adsorbent sample. From the graph it can be seen that the biochars have exhibited the highest adsorption capacities relating to both Cu^{2+} ions (WB) and MG (RH). The char samples obtained from peat and coal appeared to have worse adsorptive properties, especially in the case of peat. Besides, Cu^{2+} can be adsorbed via formation of complexes and electrostatic interaction with oxygen-containing groups [43]. Also, Cu^{2+} ions can substitute alkali and alkaline-earth metal ions to get bound by the corresponding O-containing surface species. In case of dyes, the adsorption mechanism is more complex and can include [44, 45]:

- surface adsorption in pores, when used char has a quite developed porosity;
- surface interaction with functional groups (–OH, –C–O etc.) via hydrogen bonds, van der Waals force;
- π–π stacking;
- electrostatic interactions.

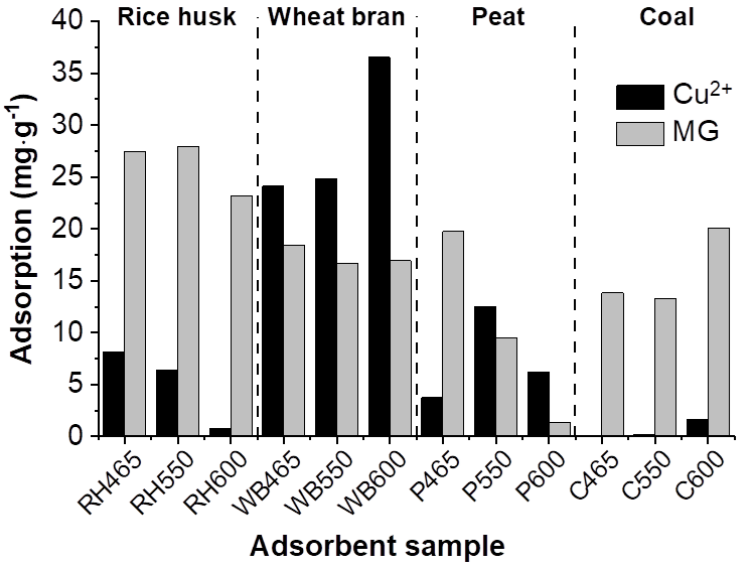

FIG. 11. Adsorption of Cu^{2+} and methyl green on the (bio)char samples obtained via carbonization in the fluidized catalyst bed reactor at 465 – 600 °C

As can be seen from the results presented in Fig. 11, adsorptive properties of the chars are weakly correlated with their BET specific surface area indicating on importance of other adsorption mechanisms. It should be noted that unlike biochars, which are usually prepared by conventional slow pyrolysis that can be conjugated with physical or chemical activation, chars prepared in this research via partial oxidation in the FCB reactor practically in all cases (except coal-derived ones) consist mainly of mineral component of the used feedstock: ash content is mostly varied from $\sim$ 50 to 80 wt. % (Table 3). Therefore, their adsorptive properties are mainly determined by ash component, and adsorption mechanisms of both transition metal ions and organic dyes apparently governed by composition and chemical properties of the mineral part. Furthermore, in the case of biochars from RH and WB, their mineral component is distributed quite homogeneously, while in the peat and coal representing sedimentary feedstocks the mineral component is distributed in the form of large agglomerates [20, 46, 47]. All the above peculiarities should be taken in consideration in discussion of the obtained results.

Copper adsorption is correlated with carbonization temperature in the case of WB and coal and inversely correlated for RH. Such dependence is apparently related to decrease in oxygen content (Table 3) with the carbonization temperature increase, except coal, when the inverse trend is observed. It is interesting to note, that WB-derived chars exhibit the highest Cu^{2+} adsorption capacity rising with the carbonization temperature, despite the drop in O-content. This most probably is caused by the highest content of alkali and alkaline-earth metals responsible for the cation exchange (see Table 2), in particularly – sodium, potassium and magnesium.

However, for the peat-derived chars, despite similar content of sodium, calcium and magnesium, their adsorption capacity is significantly worse that seems to relate with their inaccessibility for cation exchange, unlike WB derived biochars.

TABLE 3. Composition of the char samples obtained at 465 – 600 °C via oxidative carbonization in FCB reactor

Char feedstock	Temperature, °C	$W^{a\,1}$, %	$A^{d\,2}$, %	CHNS-O composition, wt. %				
				C, %	H, %	N, %	S, %	O [3], %
Rice husk	465	2.4	57.1	28.0	3.1	0.49	0.50	9.8
	550	2.3	67.8	17.0	3.0	0.45	0.50	10.6
	600	1.6	79.9	12.6	3.0	0.46	0.60	3.1
WB	465	2.7	50.9	36.0	3.6	3.80	0.45	4.0
	550	2.3	52.6	33.7	3.8	3.10	0.4	5.3
	600	2.0	58.2	32.0	4.0	2.60	0.27	2.1
Peat	465	2.0	58.5	20.3	1.9	1.34	0.29	16.9
	550	0.7	72.9	10.9	1.5	0.52	0.28	13.7
	600	0.7	79.1	7.1	1.3	0.26	0.25	11.9
Coal	465	2.4	16.5	69.2	2.9	2.17	0.29	6.9
	550	1.3	18.1	67.0	3.8	2.20	0.29	7.5
	600	1.2	19.9	63.0	3.4	2.16	0.27	10.3

[1] – moisture content; [2] – ash content on dry matter; [3] – calculated by difference

Adsorption of the MG occurs differently compared to the copper ions. Except coal-derived chars, the MG adsorption decreases with the carbonization temperature increase. This points on a certain dependence of dye adsorption on content of the carbon-containing phase forming porous structure with such adsorption sites as functional groups, aromatic rings (via π–π stacking) and others listed above. Besides, MG adsorption depends, probably, on porous structure and it is lower for the most of microporous char obtained from coal, despite they have the highest BET surface area. For coal-derived chars MG adsorption increases with carbonization temperature probably due to increase in A_{BET} and the content of oxygen being introduced onto the char surface in the carbonization process in the form of surface functional groups that play a role as one type of adsorption sites.

On the whole, the obtained results have shown that the carbon-mineral chars are promising adsorbents for both transition metal ions and organic dyes. The obtained adsorption values are comparable with those reported in many literature sources (Table 4).

4. Conclusions

A novel approach to facile, green and energy-efficient production of porous char adsorbents from the feedstocks of various nature (wheat bran, rice husk, highly-mineralized peat and coal) is proposed. It represents oxidative carbonization in fluidized bed of deep oxidation CuO–Cr_2O_3/γ-Al_2O_3 catalyst at low temperatures (465, 550 and 600 °C). This technique allowed for production of porous carbon-mineral char materials with different properties that depend on both temperature and characteristics of the used feedstocks. They appeared to have a quite high BET specific surface area (up to ~ 170 m^2g^{-1}) as well as the content of the mineral part (16 – 79 wt. %). Due to similar nature and composition, wheat bran and rice husk exhibited similar behavior and properties of the obtained biochars: their maximal BET specific surface area was reached at 550 °C (91 and 117 m^2g^{-1} correspondingly) at similar pore size distribution. Sedimentary feedstocks (peat and coal) appeared to exhibit different both combustion behavior and properties of the chars produced. Due to the high content of Ca-containing ash component and partially decomposed biomass-originated organic phase, peat-derived chars have a relatively low texture characteristics with $A_{BET} \leq\sim 10$ m^2g^{-1} at the high yield and ash content. Coal-derived chars represented the highest stability to oxidation and, correspondingly, the highest yield ($\sim$ 40 – 50 wt. %), A_{BET} (up to 172 m^2g^{-1}) as well as the lowest ash content ($\sim$ 16 – 20 wt. %).

Their adsorption properties relating to the tested adsorbates were found to be quite complex that caused by the complex adsorption mechanisms. Adsorption of Cu^{2+} ions was detected to be the highest ($\sim$ 24 – 37 mg·g^{-1}) for wheat bran due to, apparently, the highest content of alkali and alkali-earth metals available for the cation exchange. Adsorption of the organic dye depended on carbon content in the chars as well as porosity features and specific surface area. The

TABLE 4. Adsorption capacities of biomass, chars or activated carbons by Cu^{2+} and methyl green reported in literature

Feedstock	Synthesis conditions	A_{BET}, m^2g^{-1}	Ash content, wt. %	Maximal capacity ($mg \cdot g^{-1}$) by:		Ref.
				Cu^{2+}	MG	
Rice straw	Pyrolysis, 400 °C, 4 h	3.6	–	27.73	–	[48]
	Pyrolysis, 400 °C, 4 h followed by treatment with $KMnO_4$	19.4	–	71.60	–	
Spent tyres	Pyrolysis, 550 °C	–	–	∼ 47	–	[49]
Pine sawdust	Hydrothermal liquefaction at 300 °C; CO_2 activation at 800 °C	425	2.9	25.18	–	[50]
Rice husk		358	59.96	22.62	–	
Date seed	Pyrolysis, 550 °C, 3 h	104.2	12.67	26.7	–	[51]
Waste tires derived activated carbon	Activation with H_3PO_4 at 650 °C, 2 h	356	–	–	71.43	[52]
Almond shell	–	–	–	–	1.1	[53]

highest adsorption capacity by methyl green was achieved by RH-derived chars (28 $mg \cdot g^{-1}$). On the whole, chars with the most attractive properties were obtained at 550 and 600 °C.

The obtained results show that the chars produced via oxidative carbonization in fluidized catalyst bed reactor with the deep oxidation catalyst can be suitable adsorbents of both heavy metal ions and organic pollutants. Thus, the developed approach can be effectively applied for production of chars from carbon-containing feedstocks of very different nature, including sedimentary one and lignocellulosic biomass.

Appendix

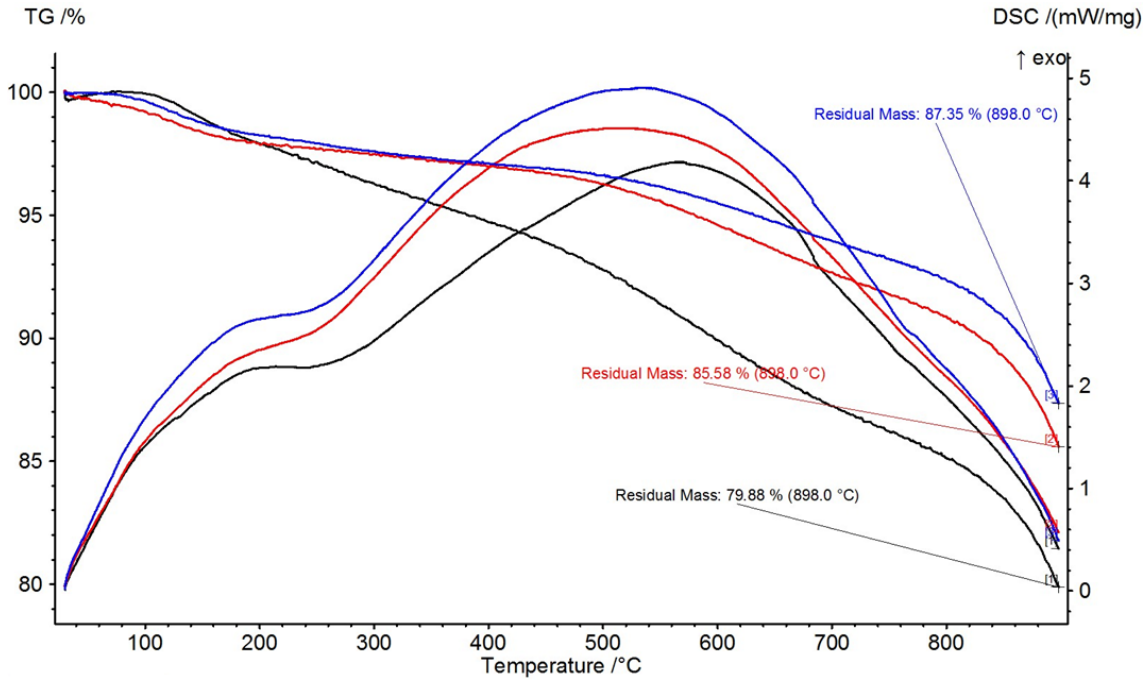

FIG. A1. TG and DSC profiles of WB-derived char samples obtained at 465 – 600 °C

TABLE A1. Texture characteristics, ash content and yield of chars from the feedstock carbonized in FCB reactor at 465 – 600 °C

Sample	A_{BET}, m^2g^{-1}	A_{EXT}, m^2g^{-1}	V_Σ, cm^3g^{-1}	V_μ, cm^3g^{-1}	$\langle d_{pore} \rangle$, nm
Bran					
B465	43	15	0.04	0.01	3.7
B550	91	40	0.05	0.02	2.2
B600	68	36	0.04	0.01	2.3
Rice husk					
RH465	87	82	0.13	0	6.0
RH550	117	102	0.17	0.01	5.8
RH600	99	78	0.18	0.01	7.4
Peat					
P465	11	11	0.05	0	19.5
P550	9	10	0.06	0	28.5
P600	7	7	0.05	0	32.7
Coal					
C465	133	61	0.07	0.03	2.1
C550	126	68	0.07	0.02	2.1
C600	172	92	0.09	0.03	2.1

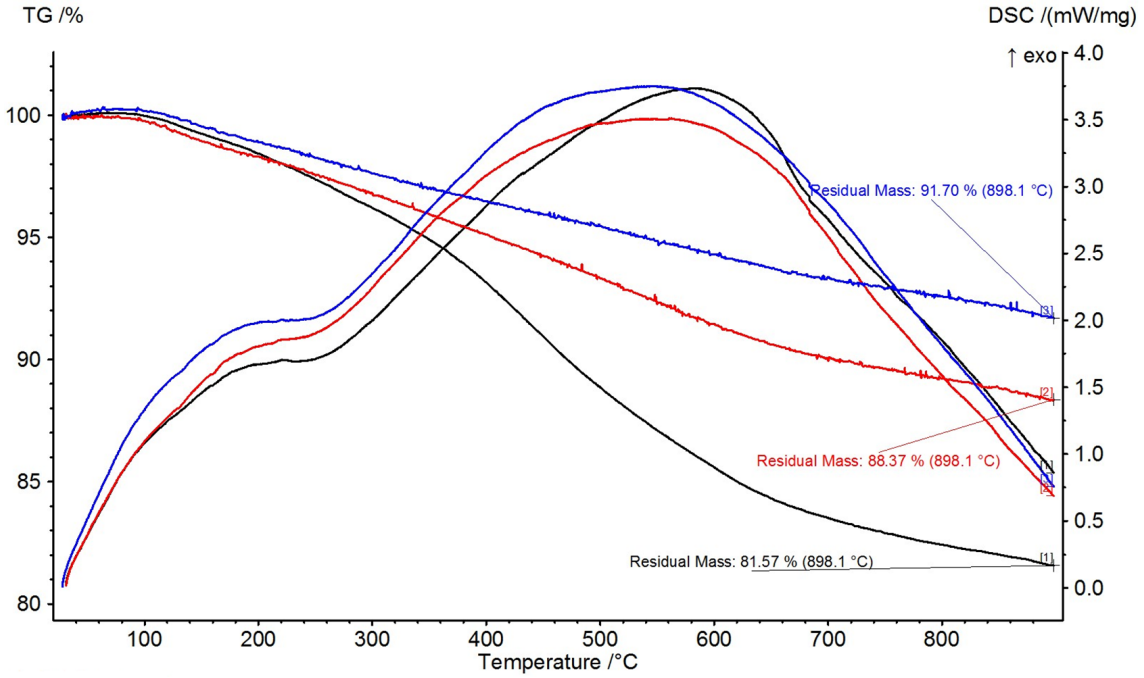

FIG. A2. TG and DSC profiles of RH-derived char samples obtained at 465 – 600 °C

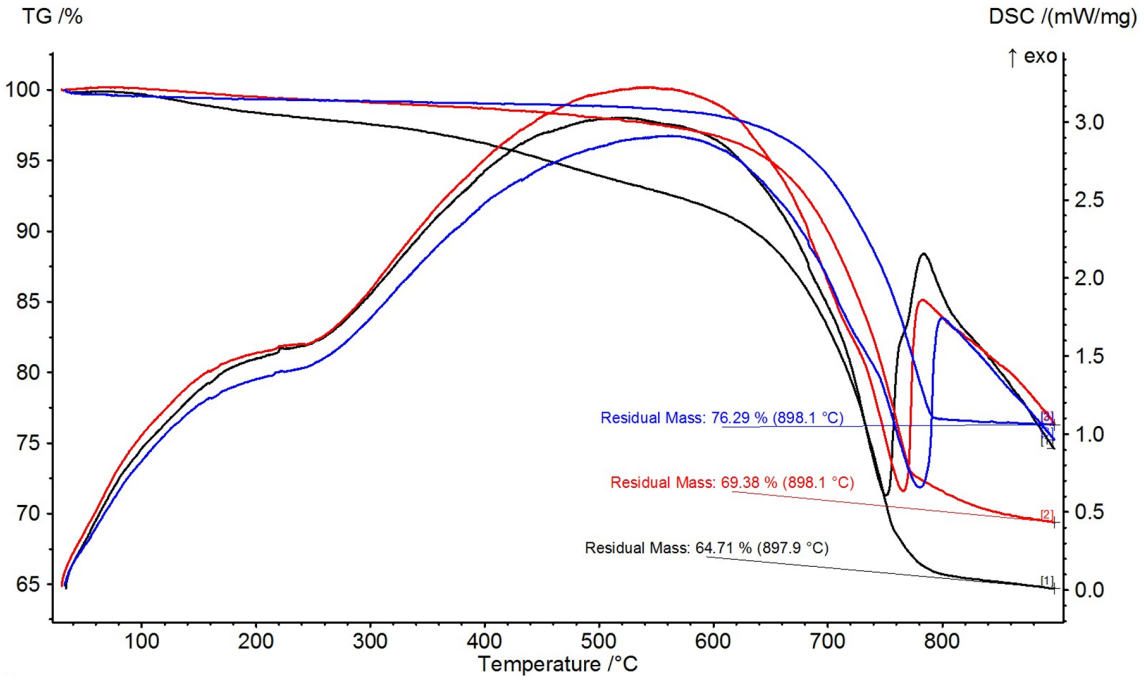

FIG. A3. TG and DSC profiles of peat-derived char samples obtained at 465 – 600 °C

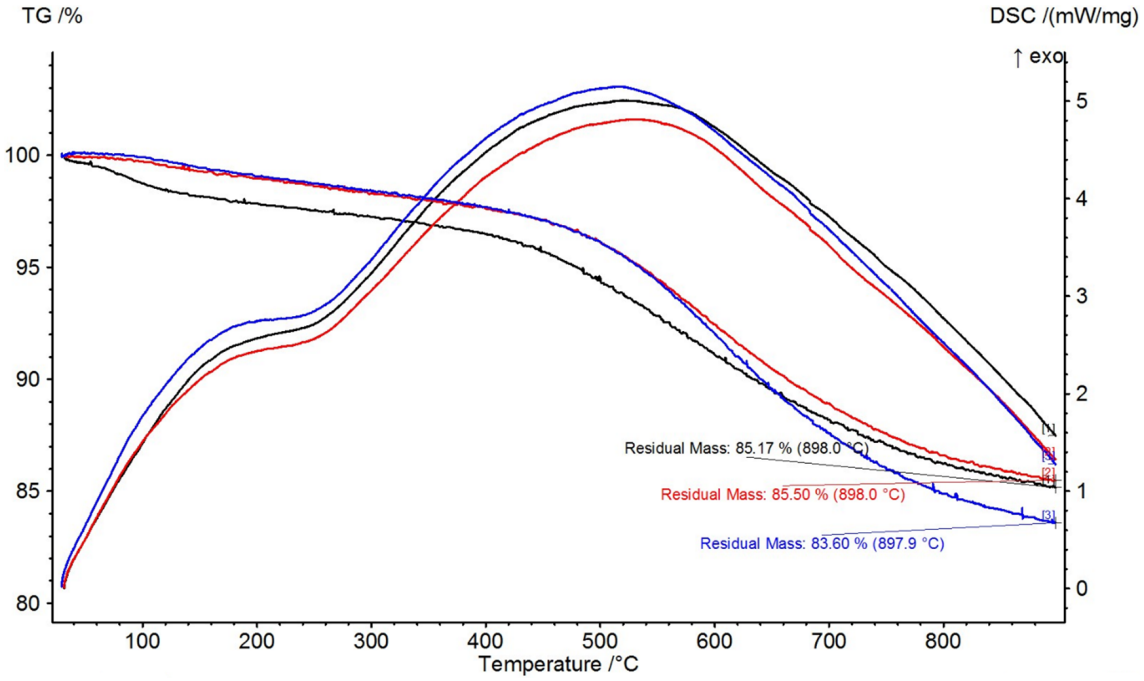

FIG. A4. TG and DSC profiles of coal-derived char samples obtained at 465 – 600 °C

References

[1] Jeguirim M., Limousy L. *Biomass Chars: Elaboration, Characterization and Applications*, MDPI, Basel, 2018.

[2] Xiang W., Zhang X., Chen J., Zou W., He F., Hu X., Tsang D.C.W., Ok Y.S., Gao B. Biochar technology in wastewater treatment: A critical review. *Chemosphere*, 2020, **252**, 126539.

[3] Suárez-Almeida M., Gómez-Barea A., Ghoniem A.F., Pfeifer C. Solar gasification of biomass in a dual fluidized bed. *Chem. Eng. J.*, 2021, **406**, 126665.

[4] Heidari M., Salaudeen S., Arku P., Acharya B., Tasnim S., Dutta A. Development of a mathematical model for hydrothermal carbonization of biomass: Comparison of experimental measurements with model predictions. *Energy*, 2021, **214**, 119020.

[5] Liu Y., Rokni E., Yang R., Ren X., Sun R., Levendis Y.A. Torrefaction of corn straw in oxygen and carbon dioxide containing gases: Mass/energy yields and evolution of gaseous species. *Fuel*, 2021, **285**, 119044.

[6] Mortari D.A., Perondi D., Rossi G.B., Bonato J.L., Godinho M., Pereira F.M. The influence of water-soluble inorganic matter on combustion of grape pomace and its chars produced by slow and fast pyrolysis. *Fuel*, 2021, **284**, 118880.
[7] Braghiroli F.L., Bouafif H., Neculita C.M., Koubaa A. Influence of Pyro-Gasification and Activation Conditions on the Porosity of Activated Biochars: A Literature Review. *Waste and Biomass Valorization*, 2020, **11**, P. 5079–5098.
[8] Li Z., Zhong Z., Zhang B., Wang W., Zhao H., Seufitelli G.V.S., Resende F.L.P. Microwave-assisted catalytic fast pyrolysis of rice husk over a hierarchical HZSM-5/MCM-41 catalyst prepared by organic base alkaline solutions. *Sci. Total Environ.*, 2021, **750**, 141215.
[9] Pawar A., Panwar N.L., Salvi B.L. Comprehensive review on pyrolytic oil production, upgrading and its utilization. *J. Mater. Cycles Waste Manag.*, 2020, **22**, P. 1712–1722.
[10] Iannello S., Morrin S., Materazzi M. Fluidised Bed Reactors for the Thermochemical Conversion of Biomass and Waste. *KONA Powder Part. J.*, 2020, **37**, P. 114–131.
[11] Karmee S.K., Kumari G., Soni B. Pilot scale oxidative fast pyrolysis of sawdust in a fluidized bed reactor: A biorefinery approach. *Bioresour. Technol.*, 2020, **318**, 124071.
[12] Mullen C.A., Boateng A.A. Accumulation of Inorganic Impurities on HZSM-5 Zeolites during Catalytic Fast Pyrolysis of Switchgrass. *Ind. Eng. Chem. Res.*, 2013, **52**, P. 17156–17161.
[13] Yazykov N.A., Simonov A.D., Dubinin Y.V., Zaikina O.O. Catalytic Co-Combustion of Peat and Anthracite in a Fluidized Bed. *Catal. Ind.*, 2019, **11**, P. 342–348.
[14] Simonov A.D., Fedorov N.A., Dubinin Y.V., Yazykov N.A., Yakovlev V.A., Parmon V.N. Catalytic heat-generating units for industrial heating. *Catal. Ind.*, 2013, **5**, P. 42–49.
[15] Yazykov N.A., Simonov A.D., Aflyatunov A.S., Dubinin Y.V., Selischeva S.A., Yakovlev V.A., Stepanenko A.I. Combustion of Shale Heavy Coal-Tar Products in a Boiling Layer of a Catalyst. *Chem. Sustain. Dev.*, 2017, **25**, P. 313–321.
[16] Yazykov N.A., Dubinin Y.V., Simonov A.D., Reshetnikov S.I., Yakovlev V.A. Features of sulfur oils catalytic combustion in fluidized bed. *Chem. Eng. J.*, 2016, **283**, P. 649–655.
[17] Dubinin Y.V., Yazykov N.A., Reshetnikov S.I., Yakovlev V.A. Catalytic combustion of sulfur-containing liquid fuels in the fluidized bed: Experiment and modeling. *J. Ind. Eng. Chem.*, 2021, **93**, P. 163–169.
[18] Fedorov A.V., Dubinin Y.V., Yeletsky P.M., Fedorov I.A., Shelest S.N., Yakovlev V.A. Combustion of sewage sludge in a fluidized bed of catalyst: ASPEN PLUS model. *J. Hazard. Mater.*, 2021, **405**, 124196.
[19] Nikitin D.S., Shanenkov I.I., Yeletsky P.M., Nassyrbayev A., Tabakaev R.B., Shanenkova Y.L., Ryskulov D.N., Tsimmerman A.I., Sivkov A.A. Agricultural waste derived silicon carbide composite nanopowders as efficient coelectrocatalysts for water splitting. *J. Clean. Prod.*, 2024, **442**, 140890.
[20] Yeletsky P.M., Dubinin Y.V., Yazykov N.A., Tabakaev R.B., Okotrub K.A., Yakovlev V.A. Conversion of natural feedstocks to porous carbons via carbonization in fluidized catalyst bed followed by leaching the feedstock mineral template phase: A comparison of biomass and sedimentary raw materials. *Fuel Process. Technol.*, 2022, **226**, 107076.
[21] Tabakaev R., Ibraeva K., Kan V., Dubinin Y., Rudmin M., Yazykov N., Zavorin A. The effect of co-combustion of waste from flour milling and highly mineralized peat on sintering of the ash residue. *Energy*, 2020, **196**, 117157.
[22] Tabakaev R., Astafev A., Dubinin Y., Yazykov N., Yakovlev V. Evaluation of Autothermal Peat Pyrolysis Realization for Fuel Processing Technologies. *Waste and Biomass Valorization*, 2019, **10**, P. 1021–1027.
[23] Yeletsky P.M., Yakovlev V.A., Mel'gunov M.S., Parmon V.N. Synthesis of mesoporous carbons by leaching out natural silica templates of rice husk. *Microporous Mesoporous Mater.*, 2009, **121**, P. 34–40.
[24] Thommes M., Kaneko K., Neimark A.V., Olivier J.P., Rodriguez-Reinoso F., Rouquerol J., Sing K.S.W. Physisorption of gases, with special reference to the evaluation of surface area and pore size distribution (IUPAC Technical Report). *Pure Appl. Chem.*, 2015, **87**, P. 1051–1069.
[25] Kruk M., Jaroniec M., Gadkaree K.P. Nitrogen Adsorption Studies of Novel Synthetic Active Carbons. *J. Colloid Interface Sci.*, 1997, **192**, P. 250–256.
[26] Liu Y., Yang X., Lei F., Xiao Y. Synergistic Effect of Alkali Metals in Coal and Introduced CaO during Steam Gasification. *J. Therm. Sci.*, 2020, **29**, P. 1627–1637.
[27] Zhao M., Memon M.Z., Ji G., Yang X., Vuppaladadiyam A.K., Song Y., Raheem A., Li J., Wang W., Zhou H. Alkali metal bifunctional catalyst-sorbents enabled biomass pyrolysis for enhanced hydrogen production. *Renew. Energy*, 2020, **148**, P. 168–175.
[28] Zhu Y., Li W., Huang Y., Zheng Y., Wang D., Ye Y., Li S., Zheng Z. Catalytic pyrolysis of cellulose over solid acidic catalysts: an environment-friendly method for furan production. *Biomass Convers. Biorefinery*, 2020, **11**, P. 2695–2702.
[29] Sosnin G.A., Yazykov N.A., Yeletsky P.M., Zaikina O.O., Yakovlev V.A. Molybdenum recovery from spent Mo-based dispersed catalyst accumulated in heavy oil steam cracking coke. *Fuel Process. Technol.*, 2020, **208**, 106520.
[30] Sing K.S.W. Reporting physisorption data for gas/solid systems with special reference to the determination of surface area and porosity (Recommendations 1984). *Pure Appl. Chem.*, 1985, **57**, P. 603–619.
[31] Jeromenok J., Weber J. Restricted Access: On the Nature of Adsorption/Desorption Hysteresis in Amorphous, Microporous Polymeric Materials. *Langmuir*, 2013, **29**, P. 12982–12989.
[32] Hanna R. Infrared Absorption Spectrum of Silicon Dioxide. *J. Am. Ceram. Soc.*, 1965, **48**, P. 595–599.
[33] Davarcioglu B., Spectral characterization of non-clay minerals found in the clays (Central Anatolian-Turkey). *Int. J. Phys. Sci.*, 2011, **6**, P. 511–522.
[34] Mozgawa W., Król M., Dyczek J., Deja J. Investigation of the coal fly ashes using IR spectroscopy. *Spectrochim. Acta Part A Mol. Biomol. Spectrosc.*, 2014, **132**, P. 889–894.
[35] Coates J. Interpretation of Infrared Spectra, A Practical Approach, in: *Encycl. Anal. Chem.*, John Wiley & Sons, Ltd, Chichester, UK, 2006.
[36] Ibrahim D.M., El-Hemaly S.A., Abdel-Kerim F.M. Study of rice-husk ash silica by infrared spectroscopy. *Thermochim. Acta*, 1980, **37**, P. 307–314.
[37] Sankar S., Sharma S.K., Kaur N., Lee B., Kim D.Y., Lee S., Jung H. Biogenerated silica nanoparticles synthesized from sticky, red, and brown rice husk ashes by a chemical method. *Ceram. Int.*, 2016, **42**, P. 4875–4885.
[38] Yin Y., Yin J., Zhang W., Tian H., Hu Z., Ruan M., Xu H., Liu L., Yan X., Chen D. FT-IR and micro-Raman spectroscopic characterization of minerals in high-calcium coal ashes. *J. Energy Inst.*, 2018, **91**, P. 389–396.
[39] Gunasekaran S., Anbalagan G., Pandi S. Raman and infrared spectra of carbonates of calcite structure. *J. Raman Spectrosc.*, 2006, **37**, P. 892–899.
[40] Mozgawa W., Król M., Dyczek J., Deja J. Investigation of the coal fly ashes using IR spectroscopy. *Spectrochim. Acta Part A Mol. Biomol. Spectrosc.*, 2014, **132**, P. 889–894.
[41] Eletskii P.M., Yakovlev V.A., Fenelonov V.B., Parmon V.N. Texture and adsorptive properties of microporous amorphous carbon materials prepared by the chemical activation of carbonized high-ash biomass. *Kinet. Catal.*, 2008, **49**, P. 708–719.
[42] He D., Ou Z., Qin C., Deng T., Yin J., Pu G. Understanding the catalytic acceleration effect of steam on $CaCO_3$ decomposition by density function theory. *Chem. Eng. J.*, 2020, **379**, 122348.

[43] Georgiou E., Mihajlović M., Petrović J., Anastopoulos I., Dosche C., Pashalidis I., Kalderis D. Single-stage production of miscanthus hydrochar at low severity conditions and application as adsorbent of copper and ammonium ions. *Bioresour. Technol.*, 2021, **337**, 125458.
[44] Yao X., Ji L., Guo J., Ge S., Lu W., Chen Y., Cai L., Wang Y., Song W. An abundant porous biochar material derived from wakame (Undaria pinnatifida) with high adsorption performance for three organic dyes. *Bioresour. Technol.*, 2020, **318**, 124082.
[45] Cuong Nguyen X., Thanh Huyen Nguyen T., Hong Chuong Nguyen T., Van Le Q., Yen Binh Vo T., Cuc Phuong Tran T., Duong La D., Kumar G., Khanh Nguyen V., Chang S.W., Jin Chung W., Duc Nguyen D. Sustainable carbonaceous biochar adsorbents derived from agro-wastes and invasive plants for cation dye adsorption from water. *Chemosphere*, 2021, **282**, 131009.
[46] Larichev Y.V., Eletskii P.M., Tuzikov F.V., Yakovlev V.A. Porous carbon-silica composites and carbon materials from rice husk: Production technology, texture, and dispersity. *Catal. Ind.*, 2013, **5**, P. 350–357.
[47] Eletskii P.M., Yakovlev V.A., Kaichev V.V., Yazykov N.A., Parmon V.N. Texture and surface properties of carbon-silica nanocomposite materials prepared by the carbonization of high-ash vegetable raw materials in a fluidized catalyst bed. *Kinet. Catal.*, 2008, **49**, P. 305–312.
[48] Meng Z., Xu T., Huang S., Ge H., Mu W., Lin Z. Effects of competitive adsorption with Ni(II) and Cu(II) on the adsorption of Cd(II) by modified biochar co-aged with acidic soil. *Chemosphere*, 2022, **293**, 133621.
[49] Shahtalebi A., Sarrafzadeh M.H., McKay G. An adsorption diffusion model for removal of copper (II) from aqueous solution by pyrolytic tyre char. *Desalin. Water Treat.*, 2013, **51**, P. 5664–5673.
[50] Liu Z., Zhang F.-S. Removal of copper (II) and phenol from aqueous solution using porous carbons derived from hydrothermal chars. *Desalination*, 2011, **267**, P. 101–106.
[51] Mahdi Z., Yu Q.J., El Hanandeh A. Investigation of the kinetics and mechanisms of nickel and copper ions adsorption from aqueous solutions by date seed derived biochar. *J. Environ. Chem. Eng.*, 2018, **6**, P. 1171–1181.
[52] Belgacem A., Brahim I.O., Belmedani M., Hadoun H. Removal of Methyl Green Dye from Aqueous Solutions Using Activated Carbon Derived from Cryogenic Crushed Waste Tires. *Iran. J. Chem. Chem. Eng.*, 2022, **41**, P. 207–219.
[53] Tanaydin M.K., Goksu A. Optimization of the adsorption of methyl green dye on almond shells using central composite design. *Desalin. Water Treat.*, 2021, **227**, P. 425–439.

Submitted 6 December 2023; revised 6 March 2024; accepted 10 March 2024

Information about the authors:

Petr M. Yeletsky – Federal Research Center Boreskov Institute of Catalysis SB RAS, Acad. Lavrentiev av., 5, Novosibirsk, 630090, Russia; ORCID 0000-0001-8899-9039; yeletsky@catalysis.ru

Nikolay A. Yazykov – Federal Research Center Boreskov Institute of Catalysis SB RAS, Acad. Lavrentiev av., 5, Novosibirsk, 630090, Russia; yazykov@catalysis.ru

Yury V. Dubinin – Federal Research Center Boreskov Institute of Catalysis SB RAS, Acad. Lavrentiev av., 5, Novosibirsk, 630090, Russia; ORCID 0000-0002-0786-0500; dubinin@catalysis.ru

Maksim M. Borodaevskiy – Federal Research Center Boreskov Institute of Catalysis SB RAS, Acad. Lavrentiev av., 5, Novosibirsk, 630090, Russia; ORCID 0009-0003-6243-5579; maxim.borodaevskiy@gmail.com

Svetlana A. Selishcheva – Federal Research Center Boreskov Institute of Catalysis SB RAS, Acad. Lavrentiev av., 5, Novosibirsk, 630090, Russia; ORCID 0000-0003-2768-9680; svetlana@catalysis.ru

Vadim A. Yakovlev – Federal Research Center Boreskov Institute of Catalysis SB RAS, Acad. Lavrentiev av., 5, Novosibirsk, 630090, Russia; ORCID 0000-0001-5015-3521; yakovlev@catalysis.ru

Conflict of interest: the authors declare no conflict of interest.